Environmental Science & Technology

pubs.acs.org/est

Article

Plasma-Generated Free Electrons Induced Perfluorooctanoic Acid Efficient Degradation at the Gas−Liquid Interface

Chengye Song, Yan Zhao, Zonghao Liu, Yueqing Zhang, Jiahao Lai, Chaoqun Tan, and Min Song*

Cite This: *Environ. Sci. Technol.* 2025, 59, 9332−9343

Read Online

ACCESS | Metrics & More | Article Recommendations | Supporting Information

ABSTRACT: Low-temperature plasma, generating both reductive electrons and diverse oxidative species, has demonstrated considerable potential for the degradation of perfluorooctanoic acid (PFOA). However, limited understanding of electron propagation mechanisms during discharge has led previous research to focus on hydrated electrons (e_{aq}^-) while neglecting free electrons (e^-). In this study, a consistent and modeled dielectric barrier discharge (DBD) plasma was employed to degrade PFOA. Contribution analysis indicated that reactions driven by e^- were dominant, with substantial contributions from hydroxyl radical (•OH)-mediated oxidation. By integrating a kinetic model with a streamer solver, a basic discharge unit model was developed. Simulation of e^- streamer propagation identified a high-intensity response electric field formed by the e^- memory effect, with a peak strength of 1.816×10^6 V/m. This electric field facilitated a secondary acceleration of e^-, allowing e^- to penetrate the surface water layer and directly attack PFOA via chain-shortening mechanisms. The delocalized state of e^- restricted degradation primarily to the gas−liquid interface, minimizing interference from the surrounding medium. This study highlights the previously overlooked role of e^- and provides essential theoretical insights for the plasma-based treatment of PFOA-contaminated water.

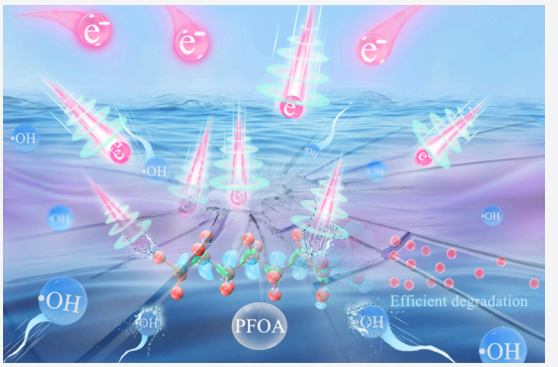

KEYWORDS: *Dielectric barrier discharge plasma, Free electrons, Perfluorooctanoic acid, Basic discharge unit model, Water treatment*

1. INTRODUCTION

Per- and poly fluoroalkyl substances (PFAS) are a group of synthetic organic compounds in which hydrogen atoms on carbon chains are fully or partially replaced by fluorine atoms.[1−3] Due to their exceptional surface activity and stability, PFAS have found extensive applications across various industries, including paper coatings, firefighting equipment, and polymer synthesis.[4,5] However, their extensive use has resulted in environmental accumulation, posing profound ecological threats.[6,7] Among these, perfluorooctanoic acid (PFOA) is particularly concerning because of its persistence, toxicity, and tendency to bioaccumulate.[8,9] The detrimental effects on reproductive, neurological, and immune systems have prompted the US Environmental Protection Agency to designate it as a persistent organic pollutant.[10,11] As a result, the search for efficient and economically viable methods to eradicate PFOA has emerged as a critical research priority.

Although physical methods, such as adsorption and membrane separation, have demonstrated effectiveness in removing PFOA, the resulting high-concentration residues necessitate additional treatment.[12] Moreover, the strong C−F bond (485 kJ/mol) poses a challenge to traditional remediation techniques. Therefore, current methods for PFOA degradation mainly encompass sonolysis,[13] thermal treatment,[14] advanced oxidation processes (AOPs),[15] and advanced reduction processes (ARPs).[16] AOPs operate through two primary mechanisms: direct disruption of molecular structures via electrochemical oxidation[17] and the generation of highly oxidative species that decompose PFOA through photocatalysis,[18] supercritical water oxidation,[19] or the addition of oxidants.[20] In contrast, ARPs focus on utilizing photochemistry effects to stimulate reducing electrons, enabling the removal or replacement of fluorine atoms with hydrogen atoms.[21] Despite the proven ability of these technologies to effectively mineralize PFOA, they are often limited by stringent experimental conditions, high reagent costs, and substantial energy consumption.[22] Recently, low-temperature plasma technology has garnered significant interest as a highly efficient approach for degrading organic pollutants without the need for external additives.[23−25] Its success in PFOA removal was particularly noteworthy, thanks to the presence of both free electrons (e^-) and hydrated electrons (e_{aq}^-), along with an array of oxidative species.[26,27]

Received: February 13, 2025
Revised: March 24, 2025
Accepted: March 25, 2025
Published: April 2, 2025

https://doi.org/10.1021/acs.est.5c02062
Environ. Sci. Technol. 2025, 59, 9332−9343

Given that hydroxyl radicals (•OH) have insufficient oxidation potential to initiate PFOA degradation, electron-dominated reduction reactions were considered as the primary mechanism.[28,29] Initially, it was assumed that e^- existed exclusively in the gaseous phase, with e_{aq}^- being regarded as the primary driving force.[30] Nevertheless, this assertion remains a subject of debate. During discharge, large amounts of nitrogen oxides were generated, releasing nitrate ions, which were potent scavengers of e_{aq}^-. Additionally, oxidizing agents and acidic conditions in the liquid phase further diminished the accessibility of e_{aq}^- to interact with contaminants.[31] Unlike photocatalysis or electrochemical methods, e_{aq}^- in plasma were primarily produced through the solvation of e^-, rather than by direct excitation in the liquid phase.[32] Recent studies indicated that e^- solvation occurred stepwise, with e^- eventually being captured by cavities formed within water molecules.[33] When the incident kinetic energy was sufficiently high, e^- could escape the water film, dissipating energy along random paths and completing solvation after reaching a certain depth.[34] Therefore, e^- may have interacted directly with PFOA at the gas−liquid interface before solvation was complete.[35] However, the absence of effective monitoring methods to track e^- generation and propagation limited discussions on their role in PFOA degradation.[36,37]

In this study, a uniform dielectric barrier discharge (DBD) plasma device was selected and optimized to evaluate its effectiveness in degrading PFOA. Through performing qualitative and quantitative analyses of reactive species and evaluating their contributions, the dominant reactive species were identified. A fluid dynamics model coupled with a parallel flow solver was employed to simulate the fundamental discharge units. This model enabled the calculation of the e^- propagation paths during discharge and the electric field density at the gas−liquid interface, enabling an in-depth discussion of the penetration effects of e^- in the aqueous phase and their accessibility to PFOA. Additionally, the degradation pathways and mechanisms of e^--initiated PFOA degradation were further investigated through density functional theory (DFT) calculations and analysis of the degradation by-products. In addition, by assessing the resistance to dielectric interference, biotoxicity, and applicability to various PFAS, we clarified the potential of the DBD system. Through elucidating the advantages of e^- in mitigating environmental interferences, valuable insights were gained regarding the application of e^--dominated plasma systems for PFOA removal.

2. MATERIALS AND METHODS

2.1. Chemicals. The degradation effects of 10 PFAS were investigated, including PFOA, perfluoroheptanoic acid (PFHpA), perfluorohexanoic acid (PFHxA), perfluoropentanoic acid (PFPeA), perfluorobutanoic acid (PFBA), perfluorooctanesulfonic acid (PFOS), perfluorohexanesulfonic acid (PFHxS), perfluorobutanesulfonic acid (PFBS), 1*H*,1*H*,2*H*,2*H*-perfluorooctanesulfonic acid (6:2 FTS), and hexafluoropropylene oxide dimer acid (GenX). In addition, five different cationic surfactants were used, namely, cetyltrimethylammonium bromide (CTAB), tetradecyltrimethylammonium bromide (TTAB), dodecyltrimethylammonium bromide (DoTAB), decyltrimethylammonium bromide (DeTAB), and octyltrimethylammonium bromide (OTAB). The analytical-grade reagents were employed without additional purification, and all solutions were prepared with deionized water (DI water) unless otherwise specified. Details were available in Text S1.

2.2. Experimental Setup. The experimental system, illustrated in Figures S1 and S2, comprised essential components including a high-voltage power supply (CTP-2000K), a pulse controller (PC-07), a voltage stabilizer (TDCG2-1), a quartz disk reactor (ϕ_{in} = 180 mm, h_{in} = 8 mm, self-designed), and an oscilloscope (Tektronix TBS-1102B). The top and bottom ends of the reactor were interfaced with a high-voltage electrode (ϕ = 120 mm) and a grounded electrode (ϕ = 100 mm), respectively. Air was introduced through a side port of the reactor, providing the necessary environment for inelastic collisions.

2.3. Experimental Procedures. In a typical pollutant removal experiment, an 80 mL solution of PFOA (10 mg/L) was introduced into the plasma reactor. After the gas flow rate was stabilized, the plasma device was powered on. At regular intervals, 50 μL of solution was collected and diluted in 3.95 mL of methanol. After ultrasonic dispersion to ensure uniform distribution of the remaining PFAS, the solution was filtered through a 0.22 μm membrane. The pollutant content in the solution was determined via liquid chromatography tandem mass spectrometry with three parallel experiments conducted for accuracy. A control experiment, with identical operational conditions except for the plasma treatment, was conducted in Figure S3. Notably, after 30 min, the concentration of PFAS in the study decreased by no more than 5%. This indicated that the potential adsorption of PFAS on the experimental setup and filter membrane did not affect the reliability of the experimental results.

2.4. Analysis Methods. The quantitative analysis of target pollutants, detection methods for intermediate products, and determination of ion concentrations are described in Text S2. The input power of the device was calculated using the Lissajous figure method.[38] The evaluation method for the degradation efficiency and the calculation method for the reaction rate constant (k_{obs}) are outlined in Text S3. The surface tension of the liquid was measured using the pendant drop method on a Dataphysics DCAT21 surface tensiometer.[39] The optical emission spectrum (OES) of the gas phase during the discharge process was measured with an AvaSpec-2048TEC spectrometer. The electron spin resonance (ESR) spectra was obtained using a Magnettech ESR 5000 instrument, with 5,5-dimethyl-1-pyrroline *N*-oxide (DMPO) employed as a spin-trapping agent. During the measurement, the following parameters were used: scan time, 60 s; microwave power, 10 mW; modulation amplitude, 2 G; and microwave attenuation, 10 dB. The method for calculating the maximum surface excess concentration is shown in Text S4. Quantitative analysis of •OH, H_2O_2, and O_3 was performed using the dimethyl sulfoxide (DMSO) method, ammonium molybdate method, and indigo carmine method, respectively. The chemical structure of PFOA was optimized using the B3LYP-6-311*G basis set in Gaussian 16.[40] The conceptual DFT descriptors, including Fukui indices, electron affinity, ionization energy, and hardness, were calculated using the Multiwfn package.[41] The biotoxicity of PFOA and its degradation products was predicted using the Toxicity Estimation Software Tool (T.E.S.T.).

3. RESULTS AND DISCUSSION

3.1. Efficiency of PFOA Degradation by DBD Plasma. After PFOA degradation and energy efficiency were evaluated,

https://doi.org/10.1021/acs.est.5c02062
Environ. Sci. Technol. 2025, 59, 9332−9343

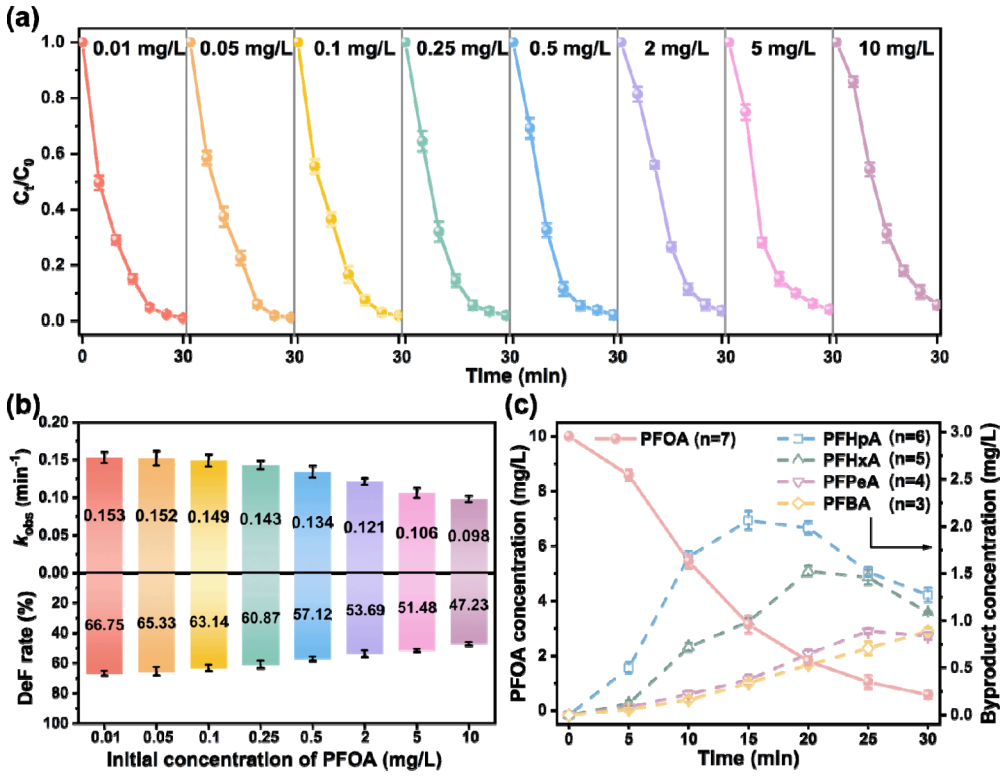

Figure 1. (a) Degradation rates, (b) k_{obs} and defluorination (deF) rates of DBD plasma for PFOA at different initial concentrations. (c) Variation in intermediate byproducts during the degradation process of 10 mg/L PFOA. System parameters: input voltage = 50 V, duty cycle = 50%, ambient temperature = 25 °C, gas environment = 30 mL/min of air.

air with a flow of 30 mL/min was chosen as the reactive medium for e^- collisions (Text S5). A pulsed power supply operating at 50 V with a 50% duty cycle was selected, delivering 21.5 W of input power (Text S7). Under the optimized conditions, the DBD plasma system effectively degraded PFOA across a wide concentration range (0.01−10 mg/L), achieving a maximum degradation rate of 98.81% (Figure 1a). Interestingly, the degradation kinetics exhibited minimal dependence on initial concentrations: the k_{obs} decreased only marginally from 0.153 to 0.098 min^{-1}, despite a three-order-of-magnitude increase in PFOA concentration (Figure 1b). Such weak concentration correlation deviated from that typically observed in a conventional homogeneous reaction, suggesting that the degradation progress was likely constrained by interfacial confinement effects. Nevertheless, even at an elevated concentration of 10 mg/L, the system accomplished a 95.05% degradation rate. Furthermore, the relatively high defluorination rate (47.23%) illustrated that the DBD system not only decomposed PFOA but also facilitated its complete mineralization.

To gain a deeper understanding of the degradation and defluorination processes, an initial PFOA concentration of 10 mg/L was selected for subsequent experiments. The temporal variations of PFOA and short-chain perfluorocarboxylic acids (PFCAs, $C_nF_{2n+1}COOH$) were measured (Figure 1c and Figure S8). With the prolongation of treatment time, the concentrations of short-chain $C_nF_{2n+1}COOH$ initially increased, peaked, and then gradually declined, a pattern typical of reaction intermediates.[42] Notably, PFPeA and PFBA, with shorter carbon chains, exhibited a slower concentration increase and later peak appearance, whereas PFHpA and PFHxA concentrations rose more rapidly. This suggested that the degradation of PFOA into shorter homologues occurred through sequential chain-shortening steps rather than random C−C bond cleavage along the chain.[43,44] Figure S9 and Table S1 compare the remediation efficacy of various treatments for PFOA-contaminated water. DBD plasma demonstrated higher k_{obs} values than electrochemical, photochemical, and persulfate activation systems, suggesting that it is a promising alternative for PFOA removal.

3.2. Detection and Contribution of Various Reactive Species. The plasma plume was analyzed in the 200−1000 nm wavelength range by using OES (Figure 2a). The detected spectral features included an OH band (298.3 and 315.6 nm), N_2 second positive system (336.6 nm), N_2^+ first negative system (357.2, 405.4, and 427.8 nm), ionized O^+ atom (375.3 and 399.2 nm), nitrogen oxide NO_X (380.2 nm), metastable O_2 ($^1\sum_g^+$, 760.2 nm), and excited-state atomic O (772.1, 869.7, and 887.8 nm). These observations confirmed the presence of abundant reactive oxygen species (ROS) and reactive nitrogen species (RNS) under excitation conditions.[45] To assess the contributions of various reactive species, a series of quenching experiments were performed (Figure 2b and Figure S10). For oxidative substances, *tert*-butanol (TBA) quenched •OH, and furfuryl alcohol (FFA) quenched both •OH and $^1O_2$, while *p*-benzoquinone (p-BQ) quenched •OH, $^1O_2$, and $O_2^{\bullet-}$. Ferulic acid (FA) was effective against $\bullet NO_2$, while uric acid (UA) quenched ONOOH. For reductive substances, NO_3^- quenched e_{aq}^-, and NO_2^- simultaneously quenched e_{aq}^- and its acidification product •H. The second-order reaction rate constants for these interactions are detailed in Table S2.

The presence of •OH scavengers notably hindered PFOA removal, with k_{obs} decreasing from 0.098 to 0.076 min^{-1}.

https://doi.org/10.1021/acs.est.5c02062
Environ. Sci. Technol. 2025, 59, 9332−9343

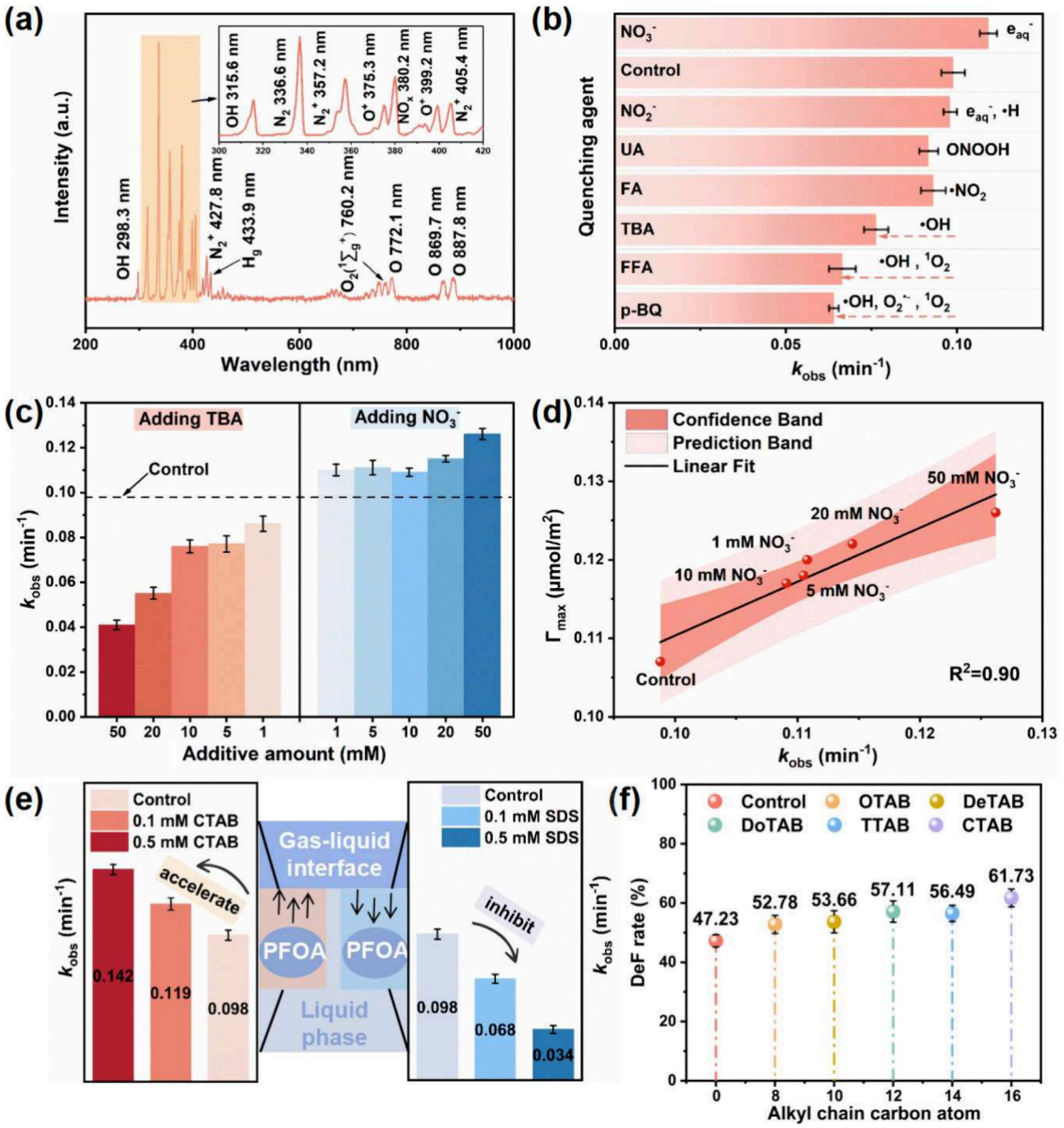

Figure 2. (a) OES signal of DBD plasma. (b) Effect of various quenchers and (c) gradient quencher dosage on PFOA degradation. (d) Correlation between k_{obs} and maximum surface excess concentration. (e) Effect of gas−liquid interface distribution on PFOA degradation and (f) impact of cationic surfactants with varying alkyl chain lengths on PFOA deF rate. System parameters: input voltage = 50 V, duty cycle = 50%, ambient temperature = 25 °C, gas environment = 30 mL/min of air, [PFOA] = 10 mg/L.

Under identical detection conditions, the addition of PFOA caused a significant reduction in the ESR signal associated with DMPO-•OH ($k_{DMPO\text{-}•OH}$ = 2.1× 10^9 M^{-1} s^{-1}), accompanied by a marked decrease in •OH concentration from 0.55 to 0.45 mM (Figure S11). This indicated that, although •OH struggled to directly cleave C−F bonds, it played a crucial role in the later stages of the multistep reaction process. The incorporation of FFA further reduced the rate to 0.066 min^{-1}, while p-BQ demonstrated analogous inhibitory effects. This implied that $^1O_2$, as a pivotal species in the free radical chain reaction, may have facilitated the degradation, whereas the contribution of the phosphorus-binding group of $O_2^{\bullet-}$ was neglected. Additionally, the minimal impact of FA and UA pointed to a relatively marginal effect of RNS. Considering the short half-lives of free radicals in water (10^{-6} to 10^{-9} s), ROS in the liquid phase primarily originated from the migration and transformation of long-lived species like O_3 and H_2O_2, rather than from direct excitation.[46] In view of the low oxidation potentials of O_3 (E_0 = 2.07 V) and H_2O_2 (E_0 = 1.78 V), which were inadequate for the direct degradation of PFOA, the decline in the levels of the O_3 and H_2O_2 upon PFOA addition implied that oxidation processes occurred both at the gas−liquid interface and within the bulk liquid phase (Figure S12). However, despite the quenching of the principal oxidants, the PFOA degradation efficiency still achieved 80.3%, suggesting that reductive processes were the predominant mechanism.

TBA could serve a protective role for e_{aq}^- by inhibiting oxidative substances.[47] However, gradient dosing experiments revealed that increasing the TBA concentration enhanced its inhibitory effect on the reaction (Figure 2c, Figures S13 and S14). In contrast, NO_3^-, as a quencher of e_{aq}^-, unexpectedly expedited the reaction,[48] with k_{obs} rising to 0.126 min^{-1}. In conjunction with the observation that NO_2^- also exhibited no inhibitory effect, it was concluded that reductants in the

https://doi.org/10.1021/acs.est.5c02062
Environ. Sci. Technol. 2025, 59, 9332−9343

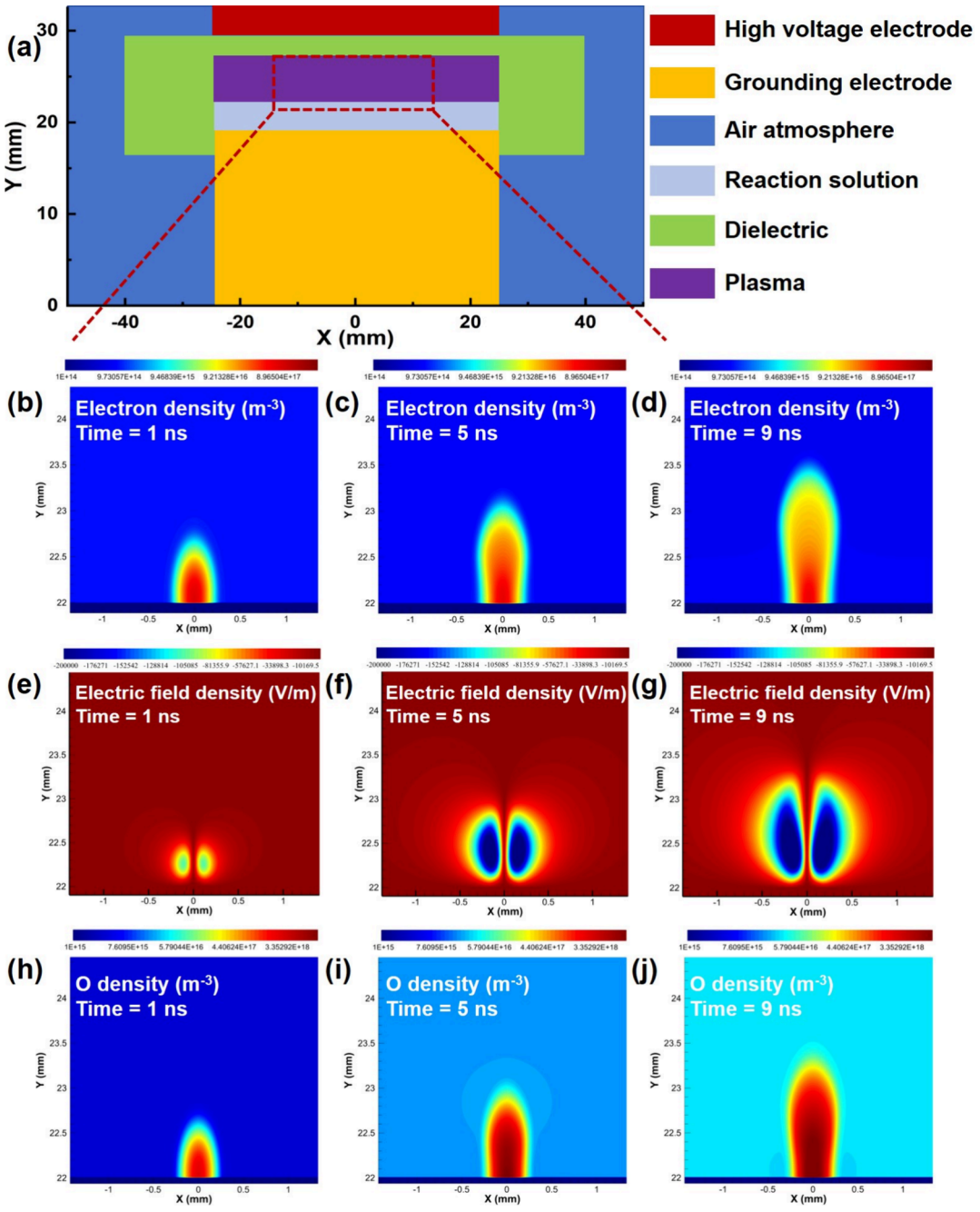

Figure 3. (a) Geometric model setup of the DBD device. Evolution of (b–d) free electron intensity, (e–g) electric field, and (h–j) oxygen density over discharge time.

solution were not effectively involved. This phenomenon could be attributed to the brief half-life of e_{aq}^- (1.0×10^{-6} s), which was readily quenched by high concentrations of dissolved oxygen, hydrogen ions, and nitrogen oxides in the solution. Furthermore, the reduction potential of •H (−2.3 V) was substantially lower than the 2.7 V required to break the C–F bond.[49] The maximum surface excess concentration (Γ_{max}) of PFOA before and after NO_3^- addition was calculated based on changes in surface tension.[50] As depicted in Figure 2d, the addition of NO_3^- led to an increase in Γ_{max}, which was strongly correlated with the enhancement of k_{obs}. Given the negligible impact of RNS, the augmentation by NO_3^- was primarily attributed to its salting-out effect,[51] which promoted the distribution of PFOA at the gas–liquid interface. Therefore, e^- accumulated at the gas–liquid interface were considered the primary driving force for PFOA degradation.

As an anionic surfactant, the interfacial distribution of PFOA was influenced by charge interactions with other surfactants.[52] Specifically, the cationic surfactant CTAB promoted the dispersion of PFOA toward the gas–liquid interface via electrostatic attraction, whereas the anionic surfactant sodium dodecyl sulfate (SDS) hindered this dispersion by forming a repulsive layer.[53] As shown in Figure 2e and Figure S15, changes in the PFOA distribution at the gas–liquid interface closely matched its degradation rate. CTAB significantly accelerated PFOA degradation with a k_{obs} value of 0.142 min^{-1}, while SDS reduced the k_{obs} value to 0.034 min^{-1}, inhibiting degradation. With increasing alkyl chain length, the

https://doi.org/10.1021/acs.est.5c02062
Environ. Sci. Technol. 2025, 59, 9332–9343

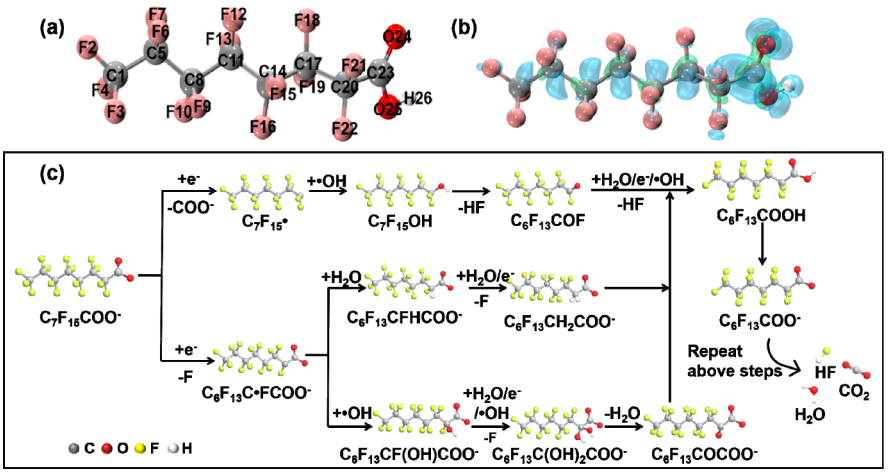

Figure 4. (a) Optimized molecular structure and (b) Fukui function (f^*) of PFOA. (c) Derived PFOA degradation pathway in the DBD system.

hydrophobicity of the quaternary ammonium compounds intensified, further promoting PFOA accumulation at the interface. At a concentration of 0.5 mM, cationic surfactants with varying alkyl chain lengths all facilitated both PFOA degradation and defluorination with the effect intensifying as the alkyl chain length increased (Figure 2f and Figure S16). This demonstrated that optimizing PFOA migration to the gas−liquid interface, thereby facilitating the mass transfer of e^- and PFOA, is a crucial strategy for improving PFOA degradation in the DBD system.

3.3. Simulation and Analysis of Propagation Paths. Given the nanosecond-scale time intervals of plasma pulse discharges, traditional diagnostic tools have faced challenges in capturing the e^- trajectory. To gain a deeper insight into the mechanisms underlying plasma generation and propagation, a 2D PASSKEy (PArallel Streamer Solver with KinEtics) code, integrated with fluid dynamics, was utilized to model the discharge unit.[54,55] The geometric setup was a 1:1 replication of the actual size (Figure 3a). Along the *Z*-axis, from bottom to top, the components were arranged as follows: ground electrode (below 19 mm), liquid layer (19−22 mm), air layer (22−27 mm), dielectric layer (27−29 mm), and high-voltage electrode (above 29 mm). Due to the combination of low pressure and short pulse duration, the influence of gas heating and expansion on the short discharge time scale was considered negligible.[56] By integrating the continuity and Poisson equations in discharge electrochemical kinetics,[57] the generation and propagation pathways of e^- and active oxygen were derived. The specific calculation method is described in detail in Text S8.

Based on the dynamics of plasma propagation, the process was categorized into four distinct phases: seed electron initiation, electron avalanche, streamer propagation, and spark discharge. In DBD plasma, dielectric materials functioned as barriers within the discharge gap, providing a stable pathway for intermittent energy input from pulsed power sources. This enabled the orderly movement and distribution of charges, leading to the formation of periodic localized discharges and preventing the transition of energy to thermal arcs. This finely controlled discharge behavior allowed the entire discharge process to decompose into a series of fundamental discharge units. Finite element simulations indicated that the discharge period lasted for approximately 9.37 ns. To more accurately capture the e^- trajectories, a single discharge cycle was selected for analysis. During the streamer propagation phase, the significantly lower mass of e^- compared with that of positive ions allowed for their rapid acceleration within the electric field, leading to charge separation. This effect was particularly pronounced at the gas−liquid interface, where it resulted in the formation of a sheath layer. The sheath electric field typically pointed toward the plasma, repelling or decelerating e^- as they approached the liquid surface. As a result, the concentration of e^- gradually increased throughout the discharge progression, with significant accumulation at the gas−liquid interface (Figure 3b−d and Figure S17).

Unlike the accumulated e^-, positive ions gradually penetrated the liquid surface, exacerbating local charge imbalances between the plasma head and tail. This imbalance, combined with the memory effect, ultimately led to the formation of a response electric field. As illustrated in Figure 3e, the response electric field bent near the interface and extended uniformly into the gas phase because of space charge effects. Under the combined influence of the response and initial electric fields, e^- began to traverse the sheath layer and move toward the liquid surface. However, due to their low kinetic energy, they were typically captured by water molecules, forming e_{aq}^-. As the surrounding electron density increased, the intensity of the response electric field correspondingly strengthened (Figure 3f,g and Figure S18), reaching a peak value of 1.816×10^6 V/m. Once sufficient kinetic energy was acquired, accelerated e^- could penetrate multiple layers of water molecules, forming radially propagating channels near or at the water surface. During this process, e^- remained in a nonsolvated, delocalized state.[58] Monte Carlo simulations showed that when the electric field strength exceeded 1×10^6 V/m,[59] the average penetration depth of plasma-generated e^- into the liquid surface reached 2.5 nm, which is significantly greater than the length of a PFOA molecule. Since the electric field generated by DBD was substantially greater than 1×10^6 V/m and water acted as the solvent, it could be inferred that e^- was able to interact with PFOA prior to solvation. Therefore, the rapid degradation of PFOA by e^- is kinetically feasible.

The generation and propagation of excited-state oxygen atoms, driven by e^- collisions, closely resembled the streamer propagation pathway (Figure 3h−j and Figure S19). The accumulated e^- led to the excitation of further oxygen atoms, which subsequently accumulated at the gas−liquid interface.

https://doi.org/10.1021/acs.est.5c02062
Environ. Sci. Technol. 2025, 59, 9332−9343

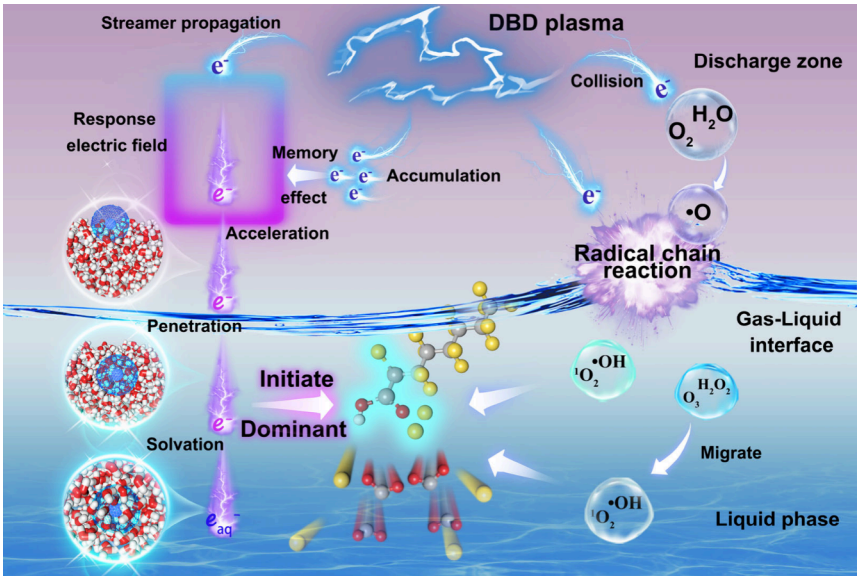

Figure 5. Schematic diagram of electron-initiated PFOA degradation in DBD plasma.

Meanwhile, oxygen atoms with higher vibrational energy levels could undergo a gradual decay process, initially transitioning from O(1D) to $O_2(b^1\sum g^+)$, and further quenching to $O_2(a^1\Delta g)$,[60] thereby avoiding direct quenching to the ground state. Under the combined effects of high-frequency excitation and stable conduction, a sufficient number of excited-state oxygen atoms reached the interface, where they reacted with water molecules through free radical chain reactions, generating ROS such as •OH, $^1O_2$, O_3, and H_2O_2.

3.4. Degradation Mechanism Initiated by e^-. In the DBD system, the PFOA degradation process did not involve random cleavage of C−C bonds, elucidating that the e^--initiated degradation mechanism was not merely a physical disintegration but rather a chemical phenomenon arising from nucleophilic attack. To predict the reactive sites of PFOA, DFT calculations were performed to determine the Fukui index (Figure 4a). Figure 4b displays the contour surfaces of the Fukui function f^+ (indicating the susceptibility to nucleophilic attack), while the condensed Fukui function index is presented in Table S3. The results indicated that C23 in the carboxyl group (f^+ = 0.1261) and O24 in the carbonyl group (f^+ = 0.1373) were the most likely reactive sites. It is noteworthy that although the f^+ value for O24 was high, the bond of O24 was saturated, making it less likely to be attacked by electrons.[61] From this, it was inferred that the carboxyl group was the preferred site for electron attack.

By identifying the reaction intermediates through UHPLC-MS and combining this with theoretical analysis (Figure S20), the degradation pathway of PFOA was proposed (Figure 4c). Given the relatively low oxidation potential of •OH, the degradation was initiated by e^- bombardment, which generated perfluoroalkyl radicals. The primary degradation and defluorination pathway in DBD was a chain-shortening mechanism, comprising decarboxylation, hydroxylation, elimination, and hydrolysis. Initially, the carboxyl group of PFOA was attacked by reductive e^-, resulting in the generation of $\bullet C_7F_{15}$. This intermediate was subsequently oxidized by •OH to yield the unstable $C_7F_{15}OH$. This compound then spontaneously lost F^- from the α-carbon, passing through the intermediate $C_6F_{13}COF$, and ultimately resulting in the production of the chain-shortened $C_6F_{13}COOH$ (PFHpA). Additionally, due to the inductive effect of the head group, the C−F bonds at the α-position near the carboxyl group exhibited higher reactivity. The high electronegativity (3.4 eV) of the fluorine atom allowed it to directly extract electrons, leading to the cleavage of the α-position C−F bond and the formation of $\bullet C_7F_{14}COO^-$. Under the influence of distinct reduction and oxidation pathways, substitution reactions primarily occurred in two forms: H/F and OH/F exchanges. After one fluorine atom on the α-position carbon was substituted, the reactivity of the remaining fluorine atom increased.[62] Consequently, the next defluorination step occurred on the same $-CF_2-$ carbon. After dual defluorination, the substitution increased the resistance of adjacent C−F bonds, making it difficult for e^--driven reductive pathways to cleave the remaining C−F bonds.[63] Fortunately, the oxidation of fluorinated end groups to PFHpA by •OH was feasible.[64] The resulting PFHpA then underwent a similar process, ultimately being mineralized through the synergistic effects of reduction and oxidation.

The degradation mechanism of PFOA via DBD plasma is summarized in Figure 5. Upon powering the device and the propagation of the plasma streamer, a significant accumulation of e^- occurred within the discharge gap, inducing a response electric field because of the memory effect. Under the secondary acceleration of this electric field, e^- gained sufficient kinetic energy to penetrate the surface water film and directly interact with PFOA at the gas−liquid interface. Simultaneously, the excited-state oxygen species at the interface generated a large quantity of •OH, which, along with e^-, constituted the primary reaction zone for PFOA degradation. In the liquid phase, the kinetic energy of e^- gradually decreased, leading to their solvation and formation of e_{aq}^-, which were quickly quenched by the surrounding environment. O_3 and H_2O_2, owing to their superior mass transfer capabilities, penetrated deeper and were further converted into •OH and $^1O_2$ through free radical chain reactions, aiding in the mineralization. By means of the synergistic effects of reduction and oxidation reactions, PFOA was gradually degraded via a chain-shortening mechanism, ultimately

https://doi.org/10.1021/acs.est.5c02062
Environ. Sci. Technol. 2025, 59, 9332−9343

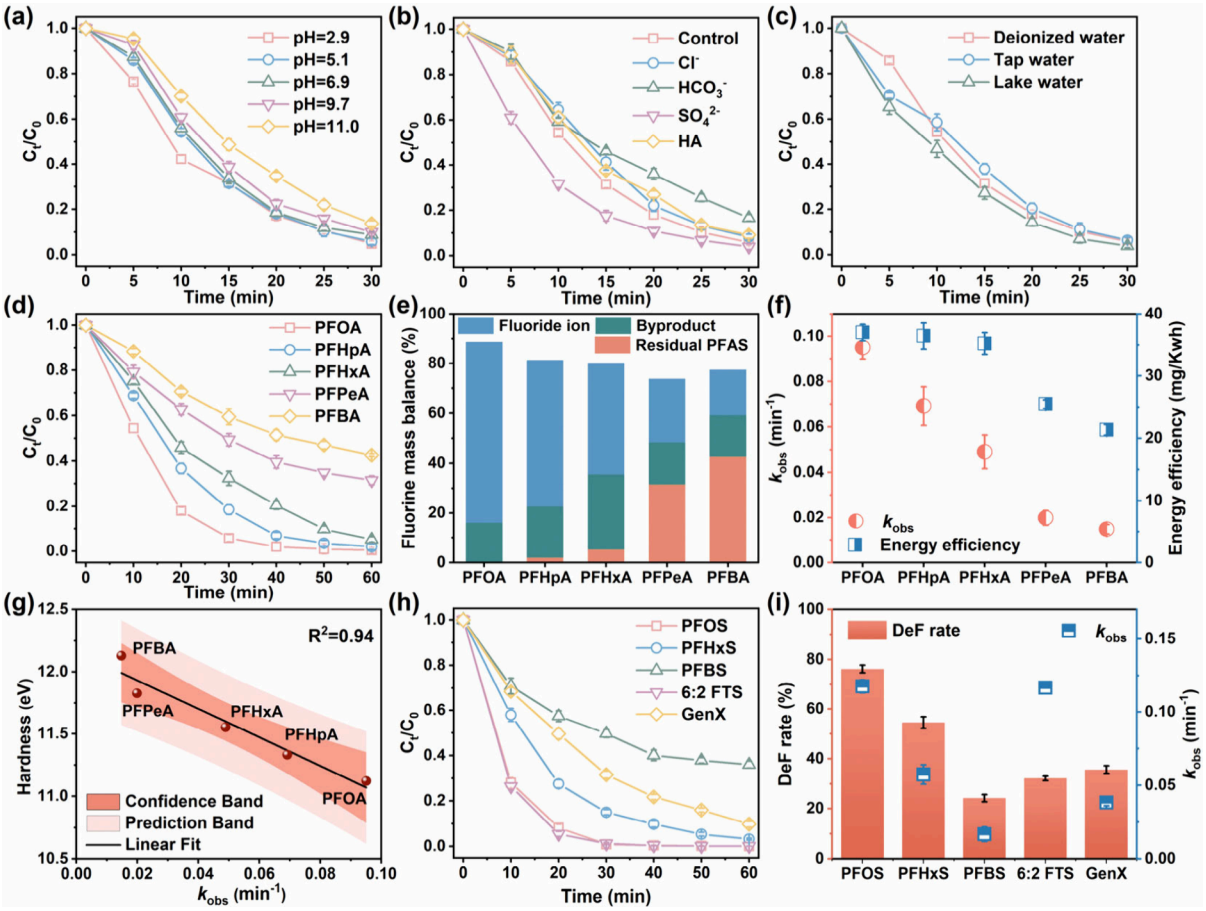

Figure 6. Effects of (a) initial pH value, (b) impurity ions, and (c) water matrix on the degradation reaction of PFOA. (d) Degradation curves, (e) fluorine mass balance, and (f) k_{obs} and energy efficiency of various PFCAs. (g) Correlation between k_{obs} and hardness. (h) Degradation curves and (i) deF rate and k_{obs} of different PFSAs as well as PFOA and PFOS substitutes. System parameters: input voltage = 50 V, duty cycle = 50%, ambient temperature = 25 °C, gas environment = 30 mL/min of air, [PFAS] = 10 mg/L.

yielding CO_2, H_2O, and free fluoride ions, achieving complete decomposition.

3.5. Assessment of Application Prospects. e_{aq}^-, constrained by hydrogen bonds with solvent molecules, were highly sensitive to the surrounding solvent environment. Conversely, e^-, owing to their delocalized nature, exhibited a reduced susceptibility to interference from the medium. Nonetheless, this inherent freedom also contributed to a certain level of instability, causing e^- to be confined to the gas−liquid interface. After identifying e^- and •OH as the main active species, we further investigated the influence of environmental factors. First, the initial pH was adjusted using 1 mol/L H_2SO_4 or NaOH. Degradation efficiency increased with decreasing pH, caused by the heightened reactivity of •OH in acidic conditions (Figure 6a). Simultaneously, PFOA, a weak acid, predominantly existed in its nondissociated form at lower pH, thereby promoting its accumulation at the gas−liquid interface. When the initial pH was adjusted to 11, the degradation rate still reached 86%. This was primarily attributed to e^-, as the main reactive species, being confined to the gas−liquid interface. Additionally, the rapid acidification of the solution minimized the impact of the initial pH. Introducing extraneous ions caused only slight inhibition, with the degradation rate reduced by no more than 11.5% (Figure 6b). The inhibitory effect of humic acid (HA) was attributed to its competition with the oxidative species. Similar to NO_3^-, SO_4^{2-} facilitated the degradation through salting-out effects.[65,66] The inhibitory effect of HCO_3^- was the most pronounced, likely resulting from its pH-buffering capacity, which facilitated the dissociation of PFOA. Moreover, HCO_3^- and Cl^- were capable of reacting with •OH, leading to the formation of species with lower oxidation potentials (•Cl and $•CO_3^-$). For both tap water and lake water (Table S4), DBD efficiently degraded over 93% of PFOA, underscoring its remarkable efficacy in practical aquatic remediation (Figure 6c). Toxicological assessments indicated that DBD treatment effectively transformed PFOA into less toxic, short-chain byproducts and liberated fluoride ions, thereby significantly mitigating its environmental hazards (Figure S21 and Table S5).

To evaluate the general applicability of DBD, the degradation performance of various PFAS was assessed. Considering the different resistances to degradation, the operation time was extended to 60 min to ensure comprehensive processing. DBD effectively removed PFCAs with varying carbon chain lengths (Figure 6d), with PFOA reaching a degradation rate of 99.6% and a defluorination rate of 72.7%. During discharge, a fraction of PFCAs protonated and decomposed into gaseous products, leading to their loss. Fluorine mass balance was calculated based on the concentrations of short-chain byproducts, fluoride ions, and residual PFAS (Figure 6e). The fluoride recovery rate

https://doi.org/10.1021/acs.est.5c02062
Environ. Sci. Technol. 2025, 59, 9332−9343

remained high, ranging from 73.8% to 88.7%, indicating that despite the possible escape of volatile byproducts such as F_2, CHF_3, and CF_4, the rapid degradation of PFCAs was primarily driven by mineralization rather than volatilization. Moreover, the degradation efficiency demonstrated a chain-length dependence (Figure 6f): as the carbon chain shortened, both the degradation rate and the energy efficiency diminished. Hardness, calculated by ionization potential and electron affinity, was indicative of the resistance to electron gain or loss. A negative correlation between k_{obs} and hardness suggested that the sensitivity to e^- played a direct role in the degradation performance (Figure 6g). Notably, while most PFCAs underwent rapid and complete degradation, PFBA and PFPeA showed a significant decrease in degradation efficiency. As reported, the length of the carbon chain significantly affected the surface polarity of PFCAs, with the Γ_{max} of PFBA being 2 orders of magnitude lower than that of PFOA.[67] This finding indicated that the distribution at the gas−liquid interface affected the efficiency of mass transfer between e^- and contaminants, thus influencing the remediation performance.

For perfluorosulfonic acids (PFSAs), a similar trend was observed with PFBS exhibiting the strongest resistance to degradation (Figure 6h). Notably, in terms of degradation rate, defluorination rate, and defluorination efficiency (Figure 6i and Figure S22), PFSAs generally outperformed PFCAs with the same carbon chain length. This enhanced performance was likely attributed to the stronger electron-withdrawing nature of the sulfonate group, which made PFSAs more susceptible to e^- attack. For the PFOA and PFOS substitutes, GenX and 6:2 FTS, DBD demonstrated high degradation rates, yet the defluorination rates remained comparatively low. This phenomenon was primarily attributed to the introduction of ether bond oxygen and hydrogen atoms. These changes altered the preferential sites for e^- attack, making the compounds more susceptible to cleavage into smaller molecules instead of gradual defluorination. Therefore, optimizing the degradation of short-chain PFAS in the DBD system constituted a pivotal challenge and a central focus for future research, as it was crucial for advancing the complete mineralization of PFAS.

3.6. Outlook. In summary, efficient PFOA degradation was achieved with DBD plasma, revealing for the first time the crucial role of previously overlooked free electrons. Simulations of electron propagation revealed the formation of a response electric field induced by the electron memory effect, which enabled electrons to penetrate the water surface and directly target PFOA. Nonsolvated, delocalized free electrons exhibited strong resilience to environmental interference, although their effect remained primarily confined to the gas−liquid interface. These findings provide novel insights for optimizing plasma-based water remediation technologies for mitigating PFOA contamination.

■ ASSOCIATED CONTENT

Supporting Information

The Supporting Information is available free of charge at https://pubs.acs.org/doi/10.1021/acs.est.5c02062.

Chemicals details; analysis methods; evaluation of pollutant degradation performance; calculation of maximum surface excess concentration; determination and optimization of working conditions; main reactions of plasma discharge under different atmospheres; modeling method for plasma field physics; diagram and image of DBD plasma device; effects of working gases, gas flow, discharge voltage, and duty cycle on the degradation of PFOA; targeted identification of various PFCAs; ESR spectra; effects of different quenchers and surfactants; variation trend of electron density, electric field, and oxygen density with discharge time; identification and toxicity assessment of degradation byproducts; comparison of the treatment effectiveness of PFOA under different processing methods; second-order reaction rates of different quenchers; Fukui index and CDD values of PFOA molecule; water quality parameters; and nomenclature and structure of PFOA and its degradation products (PDF)

■ AUTHOR INFORMATION

Corresponding Author

Min Song − *Key Laboratory of Energy Thermal Conversion and Control of Ministry of Education, School of Energy and Environment, Southeast University, Nanjing 210096, China;* orcid.org/0000-0002-0002-0568; Email: minsong@seu.edu.cn

Authors

Chengye Song − *Key Laboratory of Energy Thermal Conversion and Control of Ministry of Education, School of Energy and Environment, Southeast University, Nanjing 210096, China*

Yan Zhao − *Anhui Provincial Academy of Eco-Environmental Science Research, Hefei 230071, China*

Zonghao Liu − *Key Laboratory of Energy Thermal Conversion and Control of Ministry of Education, School of Energy and Environment, Southeast University, Nanjing 210096, China*

Yueqing Zhang − *Key Laboratory of Pesticide Environmental Assessment and Pollution Control, Nanjing Institute of Environmental Sciences, Ministry of Ecology and Environment, Nanjing 210042, China*

Jiahao Lai − *Key Laboratory of Energy Thermal Conversion and Control of Ministry of Education, School of Energy and Environment, Southeast University, Nanjing 210096, China*

Chaoqun Tan − *School of Civil Engineering, Southeast University, Nanjing 210096, China*

Complete contact information is available at: https://pubs.acs.org/10.1021/acs.est.5c02062

Notes

The authors declare no competing financial interest.

■ ACKNOWLEDGMENTS

This research was funded by the National Natural Science Foundation of China (52076043 and 52222609). Computational support was provided by the Institute of Computing Technology, Chinese Academy of Sciences, Beijing 100190, China.

■ REFERENCES

(1) Xia, D.; Zhang, H.; Ju, Y.; Xie, H.-b.; Su, L.; Ma, F.; Jiang, J.; Chen, J.; Francisco, J. S. Spontaneous Degradation of the "Forever Chemicals" Perfluoroalkyl and Polyfluoroalkyl Substances (PFASs) on Water Droplet Surfaces. *J. Am. Chem. Soc.* **2024**, *146* (16), 11266−11271.

(2) Austin, C.; Purohit, A. L.; Thomsen, C.; Pinkard, B. R.; Strathmann, T. J.; Novosselov, I. V. Hydrothermal Destruction and

Defluorination of Trifluoroacetic Acid (TFA). *Environ. Sci. Technol.* **2024**, *58* (18), 8076−8085.
(3) Li, J.; Li, X.; Da, Y.; Yu, J.; Long, B.; Zhang, P.; Bakker, C.; McCarl, B. A.; Yuan, J. S.; Dai, S. Y. Sustainable environmental remediation via biomimetic multifunctional lignocellulosic nanoframework. *Nat. Commun.* **2022**, *13* (1), 4368.
(4) Bolan, N.; Sarkar, B.; Yan, Y.; Li, Q.; Wijesekara, H.; Kannan, K.; Tsang, D. C. W.; Schauerte, M.; Bosch, J.; Noll, H.; Ok, Y. S.; Scheckel, K.; Kumpiene, J.; Gobindlal, K.; Kah, M.; Sperry, J.; Kirkham, M. B.; Wang, H.; Tsang, Y. F.; Hou, D.; Rinklebe, J. Remediation of poly- and perfluoroalkyl substances (PFAS) contaminated soils - To mobilize or to immobilize or to degrade? *J. Hazard. Mater.* **2021**, *401*, No. 123892.
(5) Zhang, Y.; Zhou, Y.; Dong, R.; Song, N.; Hong, M.; Li, J.; Yu, J.; Kong, D. Emerging and legacy per- and polyfluoroalkyl substances (PFAS) in fluorochemical wastewater along full-scale treatment processes: Source, fate, and ecological risk. *J. Hazard. Mater.* **2024**, *465*, No. 133270.
(6) Song, D.; Qiao, B.; Wang, X.; Zhao, L.; Li, X.; Zhang, P.; Yao, Y.; Chen, H.; Zhu, L.; Sun, H. Degradation of Perfluorooctanoic Acid by Chlorine Radical Triggered Electrochemical Oxidation System. *Environ. Sci. Technol.* **2023**, *57* (25), 9416−9425.
(7) Fang, Y.; Meng, P.; Schaefer, C.; Knappe, D. R. U. Removal and destruction of perfluoroalkyl ether carboxylic acids (PFECAs) in an anion exchange resin and electrochemical oxidation treatment train. *Water Res.* **2023**, *230*, No. 119522.
(8) Isowamwen, O.; Li, R.; Holsen, T.; Thagard, S. M. Plasma-assisted degradation of a short-chain perfluoroalkyl substance (PFAS): Perfluorobutane sulfonate (PFBS). *J. Hazard. Mater.* **2023**, *456*, No. 131691.
(9) Liu, Z.; Zhao, Y.; Cao, X.; Tan, C.; Wang, S.; Song, C.; Lai, J.; Wang, Z.; Song, M. High metal-loaded sub-nanocluster catalyst enhanced Fenton-like reaction activity for emerging contaminants degradation by generating high-valent copper. *Sep. Purif. Technol.* **2025**, *356*, No. 129794.
(10) Liu, Z.; Zhang, P.; Wei, Z.; Xiao, F.; Liu, S.; Guo, H.; Qu, C.; Xiong, J.; Sun, H.; Tan, W. Porous Fe-doped graphitized biochar: An innovative approach for co-removing per-/polyfluoroalkyl substances with different chain lengths from natural waters and wastewater. *Chem. Eng. J.* **2023**, *476*, No. 146888.
(11) Wang, W.; Zhang, M.; Fan, Q.; Li, C.; Li, H. Dual Role of Microbe−FexSy Interaction to Drive Perfluorooctanoic Acid Multipath Chain Reaction Decay Cycles and Secondary Minerals-Ions (Fe^{2+}/Fe^{3+}) Transformation Cycles. *ACS ES&T Water* **2024**, *4* (5), 2123−2134.
(12) Du, Z.; Deng, S.; Bei, Y.; Huang, Q.; Wang, B.; Huang, J.; Yu, G. Adsorption behavior and mechanism of perfluorinated compounds on various adsorbents–a review. *J. Hazard. Mater.* **2014**, *274*, 443−454.
(13) Sidnell, T.; Wood, R. J.; Hurst, J.; Lee, J.; Bussemaker, M. J. Sonolysis of per- and poly fluoroalkyl substances (PFAS): A meta-analysis. *Ultrason. Sonochem.* **2022**, *87*, No. 105944.
(14) Bruton, T. A.; Sedlak, D. L. Treatment of perfluoroalkyl acids by heat-activated persulfate under conditions representative of in situ chemical oxidation. *Chemosphere* **2018**, *206*, 457−464.
(15) Asadi Zeidabadi, F.; Banayan Esfahani, E.; Moreira, R.; McBeath, S. T.; Foster, J.; Mohseni, M. Structural dependence of PFAS oxidation in a boron doped diamond-electrochemical system. *Environ. Res.* **2024**, *246*, No. 118103.
(16) Bao, Y.; Deng, S.; Jiang, X.; Qu, Y.; He, Y.; Liu, L.; Chai, Q.; Mumtaz, M.; Huang, J.; Cagnetta, G.; Yu, G. Degradation of PFOA Substitute: GenX (HFPO-DA Ammonium Salt): Oxidation with UV/Persulfate or Reduction with UV/Sulfite? *Environ. Sci. Technol.* **2018**, *52* (20), 11728−11734.
(17) Teng, X.; Qi, Y.; Guo, R.; Zhang, S.; Wei, J.; Ajarem, J. S.; Maodaa, S.; Allam, A. A.; Wang, Z.; Qu, R. Enhanced electrochemical degradation of perfluorooctanoic acid by ligand-bridged Pt(II) at Pt anodes. *J. Hazard. Mater.* **2024**, *464*, No. 133008.
(18) Liu, J.; Guo, C.; Wu, N.; Li, C.; Qu, R.; Wang, Z.; Jin, R.; Qiao, Y.; He, Z.; Lu, J.; Feng, X.; Zhang, Y.; Wang, A.; Gao, J. Efficient photocatalytic degradation of PFOA in N-doped In_2O_3/simulated sunlight irradiation system and its mechanism. *Chem. Eng. J.* **2022**, *435*, No. 134627.
(19) Rosansky, S.; Al-Dirani, S. M.; Scheitlin, C. G.; Dasu, K.; Dzurnak, M.; Xia, X.; Orth, C.; McCauley, M.; Mullins, L. Field Demonstration of PFAS Destruction in Various Alcohol-Resistant AFFFs Using Supercritical Water Oxidation (SCWO). *ACS ES&T Water* **2024**, *4* (10), 4486−4496.
(20) Yang, L.; He, L.; Xue, J.; Ma, Y.; Xie, Z.; Wu, L.; Huang, M.; Zhang, Z. Persulfate-based degradation of perfluorooctanoic acid (PFOA) and perfluorooctane sulfonate (PFOS) in aqueous solution: Review on influences, mechanisms and prospective. *J. Hazard. Mater.* **2020**, *393*, No. 122405.
(21) Chen, Z.; Zhang, S.; Mi, N.; Wang, X.; Xu, Y.; Qiu, L.; Gu, C.; Zeng, G. Synergistic adsorption and UV degradation of perfluorooctanoic acid by amine-functionalized A-center sphalerite. *Water Res.* **2024**, *265*, No. 122277.
(22) Restivo, J.; Orge, C. A.; Soares, O. S. G. P.; Pereira, M. F. R. A review of current and prospective catalytic routes for the management of PFAs contamination in water. *J. Environ. Chem. Eng.* **2024**, *12* (3), No. 112859.
(23) Chen, M.; Moher, D.; Rogers, J.; Yatom, S.; Thimsen, E.; Parker, K. M. Effects of Halides on Organic Compound Degradation during Plasma Treatment of Brines. *Environ. Sci. Technol.* **2024**, *58* (11), 5139−5152.
(24) Wang, Y.; Xiang, L.; Li, Z.; Han, J.; Guo, H. Sulfite activation by water film dielectric barrier discharge plasma for ibuprofen degradation: efficiency, comparison of persulfate, mechanism, active substances dominant to pathway, and toxicity evaluation. *Sep. Purif. Technol.* **2024**, *330*, No. 125531.
(25) Su, Y.; Yang, Y.; Jiang, W.; Han, J.; Guo, H. A novel strategy of peracetic acid activation by dielectric barrier discharge plasma for bisphenol a degradation: Feasibility, mechanism and active species dominant to degradation pathway. *Chem. Eng. J.* **2023**, *476*, No. 146469.
(26) Saleem, M.; Biondo, O.; Sretenović, G.; Tomei, G.; Magarotto, M.; Pavarin, D.; Marotta, E.; Paradisi, C. Comparative performance assessment of plasma reactors for the treatment of PFOA; reactor design, kinetics, mineralization and energy yield. *Chem. Eng. J.* **2020**, *382*, No. 123031.
(27) Guo, J.; Zhang, Y.; Sun, Q.; Qu, G.; Wei, L.; Wang, T.; Jia, H.; Zhu, L. Theoretical and experimental insights into electron-induced efficient defluorination of perfluorooctanoic acid and perfluorooctane sulfonate by mesoporous plasma. *Chem. Eng. J.* **2022**, *430*, No. 132922.
(28) Papalexopoulou, K.; Huang, X.; Ronen, A.; Aggelopoulos, C. A. Reactive species and mechanisms of perfluorooctanoic acid (PFOA) degradation in water by cold plasma: The role of HV waveform, reactor design, water matrix and plasma gas. *Sep. Purif. Technol.* **2024**, *342*, No. 126955.
(29) Singh, R. K.; Fernando, S.; Baygi, S. F.; Multari, N.; Thagard, S. M.; Holsen, T. M. Breakdown Products from Perfluorinated Alkyl Substances (PFAS) Degradation in a Plasma-Based Water Treatment Process. *Environ. Sci. Technol.* **2019**, *53* (5), 2731−2738.
(30) Biondo, O.; Tomei, G.; Saleem, M.; Sretenovic, G. B.; Magarotto, M.; Marotta, E.; Paradisi, C. Products, reactive species and mechanisms of PFOA degradation in a self-pulsing discharge (SPD) plasma reactor. *Chemosphere* **2023**, *341*, No. 139972.
(31) Wei, Y.; Lu, G.; Xie, D.; Sun, T.; Liu, Y.; Zhang, Y.; An, J.; Li, M.; Guo, H. Degradation of enrofloxacin in aqueous by DBD plasma and UV: Degradation performance, mechanism and toxicity assessment. *Chem. Eng. J.* **2022**, *431*, No. 133360.
(32) Al-Zubeidi, A.; Ostovar, B.; Carlin, C. C.; Li, B. C.; Lee, S. A.; Chiang, W. Y.; Gross, N.; Dutta, S.; Misiura, A.; Searles, E. K.; Chakraborty, A.; Roberts, S. T.; Dionne, J. A.; Rossky, P. J.; Landes, C. F.; Link, S. Mechanism for plasmon-generated solvated electrons. *Proc. Natl. Acad. Sci. U.S.A.* **2023**, *120* (3), No. e2217035120.

https://doi.org/10.1021/acs.est.5c02062
Environ. Sci. Technol. 2025, 59, 9332−9343

(33) Sopena Moros, A.; Li, S.; Li, K.; Doumy, G.; Southworth, S. H.; Otolski, C.; Schaller, R. D.; Kumagai, Y.; Rubensson, J. E.; Simon, M.; Dakovski, G.; Kunnus, K.; Robinson, J. S.; Hampton, C. Y.; Hoffman, D. J.; Koralek, J.; Loh, Z. H.; Santra, R.; Inhester, L.; Young, L. Tracking Cavity Formation in Electron Solvation: Insights from X-ray Spectroscopy and Theory. *J. Am. Chem. Soc.* **2024**, *146* (5), 3262−3269.
(34) Jordan, C. J. C.; Coons, M. P.; Herbert, J. M.; Verlet, J. R. R. Spectroscopy and dynamics of the hydrated electron at the water/air interface. *Nat. Commun.* **2024**, *15* (1), 182.
(35) Brusseau, M. L. The influence of molecular structure on the adsorption of PFAS to fluid-fluid interfaces: Using QSPR to predict interfacial adsorption coefficients. *Water Res.* **2019**, *152*, 148−158.
(36) Singh, R. K.; Multari, N.; Nau-Hix, C.; Woodard, S.; Nickelsen, M.; Mededovic Thagard, S.; Holsen, T. M. Removal of Poly- and Per-Fluorinated Compounds from Ion Exchange Regenerant Still Bottom Samples in a Plasma Reactor. *Environ. Sci. Technol.* **2020**, *54* (21), 13973−13980.
(37) Stratton, G. R.; Dai, F.; Bellona, C. L.; Holsen, T. M.; Dickenson, E. R.; Mededovic Thagard, S. Plasma-Based Water Treatment: Efficient Transformation of Perfluoroalkyl Substances in Prepared Solutions and Contaminated Groundwater. *Environ. Sci. Technol.* **2017**, *51* (3), 1643−1648.
(38) Lin, C.; Liu, Z.; Zhao, Y.; Song, C.; Meng, F.; Song, B.; Zuo, G.; Qi, Q.; Wang, Y.; Yu, L.; Song, M. Oxygen-mediated dielectric barrier discharge plasma for enhanced degradation of chlorinated aromatic compounds. *Sep. Purif. Technol.* **2023**, *313*, No. 123445.
(39) Lai, J.; Liu, H.; Yang, Z.; Deng, R.; Xiong, Y.; Li, Y.; Song, M. Promotion of aromatic amino acids of extracellular polymeric substance targeted transformation via sulfite mediated iron redox cycling in sludge solid-liquid separation. *Water Res.* **2024**, *266*, No. 122369.
(40) Zhao, Y.; Zhang, B.; Xia, B.; Liu, Z.; Tan, C.; Song, C.; Fujii, M.; Ma, L.; Song, M. Defect Engineering Boosted Peroxydisulfate Activation of Dual-Vacancy Cu−Fe Spinel Oxides for Soil Organics Decontamination. *ACS ES&T Engg.* **2024**, *4* (8), 2025−2035.
(41) Lu, T.; Chen, F. Multiwfn: a multifunctional wavefunction analyzer. *J. Comput. Chem.* **2012**, *33* (5), 580−592.
(42) Singh, R. K.; Brown, E.; Mededovic Thagard, S.; Holsen, T. M. Treatment of PFAS-containing landfill leachate using an enhanced contact plasma reactor. *J. Hazard. Mater.* **2021**, *408*, No. 124452.
(43) Saleem, M.; Tomei, G.; Beria, M.; Marotta, E.; Paradisi, C. Highly efficient degradation of PFAS and other surfactants in water with atmospheric RAdial plasma (RAP) discharge. *Chemosphere* **2022**, *307*, No. 135800.
(44) Zheng, J.; Zhang, S. Subnanoscale spatially confined heterogeneous Fenton reaction enables mineralization of perfluorooctanoic acid. *Water Res.* **2023**, *246*, No. 120696.
(45) Zhang, A.; Zhou, Y.; Li, Y.; Liu, Y.; Li, X.; Xue, G.; Miruka, A. C.; Zheng, M.; Liu, Y. Motivation of reactive oxygen and nitrogen species by a novel non-thermal plasma coupled with calcium peroxide system for synergistic removal of sulfamethoxazole in waste activated sludge. *Water Res.* **2022**, *212*, No. 118128.
(46) Song, C.; Lin, C.; Zhao, Y.; Tan, C.; Liu, Z.; Song, M. Augmented degradation performance of dielectric barrier discharge plasma via optimized hydroxyl radical generation. *Sep. Purif. Technol.* **2024**, *338*, No. 126497.
(47) Biswas, S.; Yamijala, S.; Wong, B. M. Degradation of Per- and Polyfluoroalkyl Substances with Hydrated Electrons: A New Mechanism from First-Principles Calculations. *Environ. Sci. Technol.* **2022**, *56* (12), 8167−8175.
(48) Wang, T.; Qu, G.; Sun, Q.; Liang, D.; Hu, S. Evaluation of the potential of p-nitrophenol degradation in dredged sediment by pulsed discharge plasma. *Water Res.* **2015**, *84*, 18−24.
(49) Zhai, Z.; Zhang, C.; Chu, L.; Zhao, Y.; Zhou, X.; Zhang, Y. Effective defluorination of novel hexafluoropropylene oxide oligomer acids under mild conditions by UV/sulfite/iodide: mechanisms and ecotoxicity. *Water Res.* **2024**, *258*, No. 121804.
(50) Le, S. T.; Gao, Y.; Kibbey, T. C. G.; O'Carroll, D. M. Calculating PFAS interfacial adsorption as a function of salt concentration using model parameters determined from chemical structure. *Sci. Total Environ.* **2022**, *848*, No. 157663.
(51) Guo, B.; Saleem, H.; Brusseau, M. L. Predicting Interfacial Tension and Adsorption at Fluid-Fluid Interfaces for Mixtures of PFAS and/or Hydrocarbon Surfactants. *Environ. Sci. Technol.* **2023**, *57* (21), 8044−8052.
(52) Li, R.; Isowamwen, O. F.; Ross, K. C.; Holsen, T. M.; Thagard, S. M. PFAS−CTAB Complexation and Its Role on the Removal of PFAS from a Lab-Prepared Water and a Reverse Osmosis Reject Water Using a Plasma Reactor. *Environ. Sci. Technol.* **2023**, *57* (34), 12901−12910.
(53) Wang, Y.-X.; Kornev, I.; Wei, C.-H.; Preis, S. Surfactant and non-surfactant radical scavengers in aqueous reactions induced by pulsed corona discharge treatment. *J. Electrost.* **2019**, *98*, 82−86.
(54) Zhu, Y.; Shcherbanev, S.; Baron, B.; Starikovskaia, S. Nanosecond surface dielectric barrier discharge in atmospheric pressure air: I. measurements and 2D modeling of morphology, propagation and hydrodynamic perturbations. *Plasma Sources Sci. Technol.* **2017**, *26* (12), No. 125004.
(55) Mao, X.; Zhong, H.; Zhang, T.; Starikovskiy, A.; Ju, Y. Modeling of the effects of non-equilibrium excitation and electrode geometry on H_2/air ignition in a nanosecond plasma discharge. *Combust. Flame* **2022**, *240*, No. 112046.
(56) Yin, B.; Zhu, Y.; Wu, Y. Modulating sparks in a pulse train for repetitive and energy efficient plasma generation. *High Volt.* **2023**, *8* (6), 1168−1179.
(57) Deng, R.; He, Q.; Yang, D.; Chen, M.; Chen, Y. Dielectric barrier discharge plasma promotes disinfection-residual-bacteria inactivation via electric field and reactive species. *Water Res.* **2024**, *254*, No. 121386.
(58) Gao, L.; Bu, Y. Competitive Hydration Versus Migration of Pre-hydrated Electrons for CO_2 Reduction in Aqueous Solution Revealed by Ab Initio Molecular Dynamics Simulation. *Adv. Theor. Simul.* **2023**, *6* (12), No. 2200938.
(59) Rumbach, P.; Bartels, D. M.; Sankaran, R. M.; Go, D. B. The solvation of electrons by an atmospheric-pressure plasma. *Nat. Commun.* **2015**, *6* (1), 7248.
(60) Xin, Z.; Zheng, Z.; Hu, Y.; Sun, A.; Zhao, F.; Yu, W. Numerical modeling of plasma assisted ignition of CH_4/O_2/He mixture by the nanosecond repetitive pulsed surface dielectric barrier discharge. *Fuel* **2024**, *357*, No. 129975.
(61) Wang, X.; Si, D.; Li, Y.; Chen, N.; Fang, G.; Zhu, C.; Zhou, D. Alcohols radicals can efficiently reduce recalcitrant perfluorooctanoic acid. *Water Res.* **2023**, *245*, No. 120557.
(62) Wang, Z.; Jin, X.; Hong, R.; Wang, X.; Chen, Z.; Gao, G.; He, H.; Liu, J.; Gu, C. New Indole Derivative Heterogeneous System for the Synergistic Reduction and Oxidation of Various Per-/Polyfluoroalkyl Substances: Insights into the Degradation/Defluorination Mechanism. *Environ. Sci. Technol.* **2023**, *57* (50), 21459−21469.
(63) Yuan, Y.; Feng, L.; He, X.; Wu, M.; Ai, Z.; Zhang, L.; Gong, J. Nitrate promoted defluorination of perfluorooctanoic acid in UV/sulfite system: Coupling hydrated electron/reactive nitrogen species-mediated reduction and oxidation. *Environ. Pollut.* **2022**, *313*, No. 120172.
(64) Liu, Z.; Bentel, M. J.; Yu, Y.; Ren, C.; Gao, J.; Pulikkal, V. F.; Sun, M.; Men, Y.; Liu, J. Near-Quantitative Defluorination of Perfluorinated and Fluorotelomer Carboxylates and Sulfonates with Integrated Oxidation and Reduction. *Environ. Sci. Technol.* **2021**, *55* (10), 7052−7062.
(65) Le, S.-T.; Gao, Y.; Kibbey, T. C. G.; Glamore, W. C.; O'Carroll, D. M. Predicting the impact of salt mixtures on the air-water interfacial behavior of PFAS. *Sci. Total Environ.* **2022**, *819*, No. 151987.
(66) Zhang, Y.; Zhang, H.; Zhang, A.; Héroux, P.; Sun, Z.; Liu, Y. Remediation of atrazine-polluted soil using dielectric barrier discharge plasma and biochar sequential batch experimental technology. *Chem. Eng. J.* **2023**, *458*, No. 141406.

https://doi.org/10.1021/acs.est.5c02062
Environ. Sci. Technol. 2025, 59, 9332−9343

(67) Zhang, H.; Zhu, L.; Zhang, Y.; Heroux, P.; Cai, L.; Liu, Y. Removal of per- and polyfluoroalkyl substances from water by plasma treatment: Insights into structural effects and underlying mechanisms. *Water Res.* **2024**, *253*, No. 121316.

https://doi.org/10.1021/acs.est.5c02062
Environ. Sci. Technol. 2025, 59, 9332−9343